

Improved Explosion Consequence Analysis with Combined CFD and Damage Models

Arno Klomfass, Alexander Stolz, Stefan Hiermaier

Fraunhofer Institute for High-Speed-Dynamics, Eckertr.8, 79104 Freiburg, Germany
 klomfass@emi.fraunhofer.de

The most-widely used approach to explosion consequence analysis is the classical engineering method based on the combination of TNT equivalence, scaled distances and overpressure-based damage levels. This approach rests on established and easily comprehensible elements and permits a fast assessment of explosion consequences. There are however several limitations inherent in this approach. In contrast, a simulation-based approach using computational fluid dynamics (CFD) and structural dynamics (CSD) methods permits an analysis with a high level of detail regarding both the prediction of the explosive loads and the caused damage. This comes at the cost of complex simulation models which require expert knowledge, intense validation and a high computational effort. To bridge the gap between the classical simplified approach and the CFD/CSD based methods, we have developed a specialized CFD tool, the APOLLO Blastsimulator, with a built-in library of experimentally validated damage models and blast-injury models suitable for an improved explosion consequence analysis. The high resolution CFD tool uses globally and locally adaptive Cartesian grids and includes models for TNT detonations as well as gas detonations. The built-in damage models are based on experimentally validated single-degree-of-freedom (SDOF) representations of structural components. This paper gives a brief review on the classical approaches and their limitations and an overview on the concepts used in the APOLLO Blastsimulator and the SDOF damage models. For an exemplary explosion scenario the results obtained with different explosive source and damage models are compared.

1. Introduction

The objective of any explosion consequence analysis is to provide conservative estimates of the physical damage caused to both the built environment and persons. It typically consists of a sequential evaluation of distinct physical models related to the different processes following the initial failure. These processes are: a) the release of the flammable substance, b) its dispersion in the ambient air, c) the vapour cloud explosion, and d) the structural response of the loaded objects and the resulting damage or injury of exposed persons. Further hazards which may have to be considered are the dispersion of toxic combustion products or the fragment throw generated by the explosion. In the following we focus on the determination of the explosive loads and the assessment of the damage of explosively loaded buildings. For both topics there is a spectrum of different methods ranging from classical simplified approaches to advanced simulation-based methods.

2. Methods for Explosive Loads Calculation

2.1 TNT Equivalent

This method makes use of empirical correlations for blast waves generated by spherical TNT detonations in the free field, (Kinney, 1985). These correlations render the peak overpressure and further blast wave properties as functions of the Hopkinson-scaled distance, $R/(M_{TNT})^{1/3}$. The equivalent TNT mass of a vapour cloud explosion (VCE) can be estimated through:

$$M_{TNT} = \eta M_f q_f / q_{TNT}, \quad (1)$$

where M_f is the mass of the combustible fuel in the vapour cloud formed by the released substance and q_f is the specific heat of combustion of the stoichiometric fuel-air mixture per mass of fuel. The energy of

detonation of TNT, q_{TNT} , is about 4.5 MJ/kg and the adjustable factor η gives the yield of the VCE. The yield depends on the mode of explosion and the actual amount and distribution of oxidizer (air) in the vapour cloud. It approaches zero for low speed free field deflagrations and can theoretically attain one for the detonation of a uniform stoichiometric cloud. From post-incident analysis a typical value range has been determined to be 0.05 - 0.1, (CPR, 2005). Under the assumption that high speed deflagrations or detonations preferentially develop in confined or obstructed parts of a vapour cloud and low speed deflagrations hardly generate overpressures the equivalent TNT mass can also be estimated by:

$$M_{TNT} = \text{Min}(V_{con}, V_{cloud}) \varepsilon_f / q_{TNT} \cdot \quad (2)$$

Here ε_f denotes the volume specific combustion energy, which is about 3.5 MJ/m³ for most hydrocarbons mixed stoichiometrically with air, and V_{con} is the confined or obstructed volume, (CPR, 2005).

The application of the TNT based correlations is limited to the far field of an explosion, as in the near field the blast waves of TNT detonations and VCE's differ significantly: the VCE produces smaller overpressures but larger overpressure impulses than the equivalent TNT detonation. For example, the TNT equivalence of stoichiometric hydrogen-air detonations is about 22.5 kg(TNT)/kg(H₂), (Klomfass 2014), which corresponds to a yield factor η of about 0.72. For this equivalence value, the peak overpressures generated by the detonation of a spherical, stoichiometrically mixed hydrogen-air cloud approaches those generated by the equivalent TNT detonation only for scaled distances above about 4 m/kg^{1/3} (TNT mass); for the overpressure impulses the values become identical at distances above about 2 m/kg^{1/3} (TNT mass), (Klomfass 2014).

2.2 VCE Blast Curves

The methods developed by Baker, Strehlow and Tang (BST) and the Multi-Energy-Method (ME) both rely on numerically computed overpressure transients for spherical VCE's of a combustible model gas stoichiometrically mixed with air under the assumption of a constant flame speed (Baker, 1996), (CPR, 2005). The computed transients were generalized by the application of scaling laws. The generalized curves provide the peak overpressure and further blast properties as functions of the Sachs-scaled distance $R/(E_{ex}/\rho_0)^{1/3}$ and a further parameter. The further parameter is either the constant flame speed (BST) or an empirical explosion severity level between 1 and 10 with 10 referring to a detonation (ME). The selection of an appropriate severity level or flame speed requires an assessment of the degree of confinement, obstruction and fuel reactivity, (CPR, 2005). The energy E_{ex} used in the scaled distance is the total heat of combustion of the gas cloud or the relevant part of it (the confined or obstructed volume). For flame speeds above the sound speed or severity levels above 6 the respective sets of blast curves converge into a single curve for Sachs-scaled distances above about 1 (BST) or 2 (ME). This means that fast deflagrations and detonations produce the same blast wave in some distance to the explosion. Above these distances the BST and ME blast curves become practically identical with the TNT based blast curves. The VCE blast curves overcome the limitation to the far field inherent in the TNT equivalence method and permit to consider non-detonative explosion events. They do however not overcome the simplification to spherical or hemispherical propagation in the free field.

2.3 Reflection Coefficients

As the above mentioned methods assume spherical symmetry, the true cloud shape must be approximated by either a sphere at some height or a hemisphere on the ground. In the latter case the equivalent TNT mass or explosion energy used for the calculation of the scaled distance is twice the value of the actual cloud. This corresponds to a ground reflection factor of two. In (CPR, 2005) it is recommended to use a reflection factor of two when the vertical elevation of the explosion centre is less than 15 degree above the loaded object and a factor one otherwise.

As the correlations for the blast properties refer to propagation in the free field, the interaction of the blast wave with the loaded object must be explicitly evaluated. If a loaded surface faces the explosion centre a normal reflection can be assumed to obtain a conservative estimate of the exerted load. For this purpose the side-on overpressure provided by a free field correlation must be multiplied by the reflection factor, (Kinney),

$$f_{refl} = (8 \Delta p_{peak} + 14 p_{amb}) / (\Delta p_{peak} + 7 p_{amb}) \cdot \quad (3)$$

The same factor is to be applied to the overpressure impulse. This factor can be approximated by the limiting value of two if the peak overpressure Δp_{peak} in the free field falls below about 10 kPa. For an improved estimate the correlation between the reflection factor and the incident angle given in (UFC, 2008) can be used. For surfaces not facing the explosion centre the free-field values may be used as reasonable approximations.

2.4 Improved Explosive Load Calculation

An improved consequence analysis should retain on the safe side but avoid unrealistic, over-conservative predictions. This can be achieved by including as much details in the analysis, as can be reliably gathered and modelled. With respect to the explosive loads these are the geometrical details of the plant and at least

approximately the height and shape of the vapour cloud (to be obtained from release- and dispersion-analysis models). These details can be easily included and reliably modelled in a CFD simulation. Thereby the actual ground reflection, the potentially non-spherical wave propagation past the multiple objects on the site and the actual wave reflection on the buildings are implicitly taken into account. The CFD simulation becomes particularly trustworthy, if established explosive source models can be used, i.e. TNT detonations and VCEs replicating the BST or ME blast curves. This permits the application of these commonly accepted models with an increased level of geometric detail and also offers a convenient basis for the validation of the simulation method. A particular aspect to be considered in the application of a CFD simulation is the influence of the finite spatial resolution on the residual error. Resolution independent, i.e. converged results are often difficult to achieve, particularly for the peak overpressure.

The APOLLO Blastsimulator (www.emi.fraunhofer.de/produkte/apollo-blastsimulator) is a CFD tool which has been specifically developed for applications in the field of explosions and blast waves. The basic models and the main features of the APOLLO Blastsimulator can be summarized as follows:

- Conservation equations for transient flows of reactive mixtures of compressible, inviscid fluids
- Chapman-Jouguet detonation model for solid explosives and non-uniform gas mixtures
- 2nd order finite volume scheme with explicit time integration in 1D and 3D
- Multi zone Cartesian grids with dynamic mesh adaption (global adaption and local refinement)
- Lagrangian model for combustible particle phases
- Solid objects modelled as embedded voxel approximations (import from CAD model)
- Variety of structural damage and blast injury models

The dynamic mesh adaption is based on a uniform discretization into large cuboid zones. Into each of these zones a uniform Cartesian grid with time variable resolution is embedded. The resolution is determined automatically from the time-dependent, zone specific gradients of pressure, temperature, density, Mach number and concentrations. Geometrical objects such as buildings are included as embedded voxel models on the highest, user selected resolution level. Zones which contain embedded objects are excluded from the dynamic adaption to ensure a persistent geometry. During the simulation the peak overpressures and the maximum overpressure impulses are recorded on all solid surfaces in the computational mesh. This permits the evaluation of overpressure/impulse based damage models (SDOF models) in a simple postprocessing operation. Presently included are models for float glass, hardened glass, laminated safety glass, masonry and reinforced concrete walls and several blast injury models. For the evaluation of higher-order damage models local or area averaged overpressure transients can be recorded on selected positions or selected surfaces.

3. Structural Damage Assessment

3.1 Methods based on explosive Strength

The simplest approaches are based on forensically derived correlations for an overall building damage with TNT equivalent and distance, c.f. Stone (2006), Gilbert (1994) and Jarrett (1968). To the same category belong the thresholds for the peak overpressure specified for certain building types, as suggested by (Pigler, 1976) or as given in (Kinney, 1985). These approaches are effective to obtain a fast first assessment of the damage for a given scenario. The accuracy is however limited and conservatism cannot be taken for granted.

3.2 Dynamic Load Factor Analysis

Equivalent static loads are used to design and evaluate the resistance of building components under blast loading by defining a static pressure which stresses the component to the same deflection than the actual dynamic load. The equivalent static load is defined through a dynamic loading factor (DLF) which depends on the waveform of the loading and the eigenfrequency of the regarded component and is thus specific for each component and each loading case. DLF definitions for explosive loading types can be found in Teich (2010); the actual design of a component can be conducted following standard regulations like EC6 for masonry constructions (Eurocode 6, 2012). If the DLF and the static loading capacity of a component are known they can be compared with the exerted dynamic peak overpressure to assess the safety of the component.

3.3 Single Degree of Freedom Models

Single-Degree-of-Freedom (SDOF) models are commonly used for the design of building components against terroristic attacks with explosives devices (Morison, 2006). They are likewise suited for application in an explosion consequence analysis in the process industry. The SDOF model relates the dynamic response, i.e. the time dependent deflection of a structural component to an arbitrary time dependent loading. For a simplistic waveform, e.g. triangular or exponentially decaying, the loading can be fully characterized by the peak overpressure and the overpressure impulse. Different combinations of these values may lead to identical deflection amplitudes of the structure. These combinations of values can be represented by an iso-curve in an overpressure-impulse diagram (c.f. figure 3 as an example). If the deflection amplitude is large enough to

cause structural damage, e.g. plastic deformation or failure, the respective curves are iso-damage curves. By comparing the actual loading in terms of peak overpressure and overpressure-impulse with such an iso-damage curve a fast classification of the structural response can be obtained: if the point representing the actual loading in the diagram is localized under the regarded iso-damage curve the respective damage will not be reached, otherwise the respective damage will be exceeded. Iso-damage curves thus permit a differentiated assessment of the expected damage. A critical review of SDOF models showed, that their validity strongly depends on the resistance function which characterizes the deflection of the component. The resistance function following Stolz (Stolz, 2014) has proven adequate for many applications. The parameters of this function are related to physical properties of the component and can be identified with an inverse calculation method from experimental test data. The inverse calculation method allows the calibration of an SDOF model with just three experimental tests in a suitable shock tube facility (Fischer, 2009). Through scaling the experimentally derived iso-damage curves can also be transferred to identical components with other dimensions. The validity of the scaling method is shown in (Stolz, 2014). As an example figure 3 shows the comparison between experimentally obtained damage levels and predictions from a SDOF model for masonry walls. It is worthwhile to note, that SDOF models may also be extended to model the effects of various retrofitting measures.

4. Example Application and Conclusions

Figure 1 shows a top view of the fictitious configuration investigated in the present study. It consists of several buildings with closed facades, three production facilities, which are here represented as porous structures, some pipeline bridges and tanks. The configuration has been conceived to demonstrate the advantages of an improved explosion modelling and also to illustrate the challenge of grid convergence. The explosion scenario studied for this purpose assumes a release of 44 kg gaseous hydrogen (a TNT equivalent of ca. 1000 kg) in a straight vertical plume at the marked position. A detailed evaluation of the explosive loads was performed for the three points on the façade of the considered building as shown at the right side of figure 1. The building is about 12 m and 16 m high in different sections. The distance of gauge 1 to the release point is ca. 260 m. It has a direct line-of-sight to the release point, while the other gauges 2 and 3 lie in the shade of the upstream located building, which has a maximum height of 24 m.

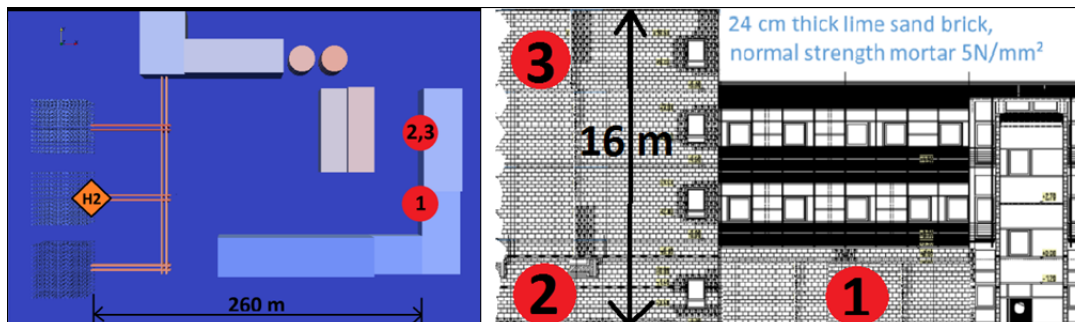


Figure 1: Left: Top view of the fictitious site with positions of hydrogen release and gauge points on the considered building; Right: Front view of the considered building with gauge positions.

The following nominally identical explosion sources (44 kg H₂, 1000 kg TNT) have been simulated:

- A Hemispherical TNT explosion on the ground (ground reflection factor 2)
- B Spherical TNT explosion centred 60 m above the release point (assumed ignition point of the VCE)
- C Detonation of a vertical, cone shaped vapour cloud with height 75 m and top side radius 4.8 m; uniform stoichiometric mixture at ambient conditions (1 bar, 288 K); ignition on centreline at 60 m height
- D Detonation of a vertical, plume shaped vapour cloud with height 75 m and max. radius 25 m; axial and radial Gaussian distribution of hydrogen concentration ranging from 100% to 0%, ignition point as in C.

A grid convergence study was conducted for model A: four simulations with different resolutions were run to 1.5 s real time. The results for gauge 1 are summarized in table 1. This gauge was selected for presentation as it allows a reasonable comparison with the correlations for the free field propagation and normal reflection. The results indicate that the overpressure impulse converges rapidly with increasing resolution, while a very high resolution is required to capture the peak overpressure at the considered gauge. With the dynamic mesh adaption method the required resolutions (several million cells) can practically be realized on a standard PC. The CPU time is still large but will be reduced in future through parallelization for modern multi-core CPUs.

Table 1: Model A simulations with different resolutions: performance, loads at gauge 1

Resolution [m]	2.5	1.25	0.625	0.3215	Empirical (Kinney)
CPU time (1 core) [h]	0.25	2	19	255	-
Average Cells/1000	200	1000	7500	55000	-
Peak OP [kPa]	3.9	6.3	8.1	9.2	8.7
Max. OP-impulse [Pa s]	185	237	233	230	234

Table 2 summarizes the results obtained with 0.625 m resolution for the different, nominally identical explosion source models. For all models it is found that the loads clearly differ for the individual gauges, although their distances to the explosion centre are nearly identical. This is due to the partial shielding of the gauges 2 and 3 by the upstream located building and the different wave reflection angles at the gauges 2 and 3. Granted that the assumed plume model is valid, model D can be regarded as the closest approximation to the real scenario. It is still conservative as the explosion was assumed to be detonative: the flame speed equals the concentration dependent CJ detonation velocity in this model (Klomfass, 2014). The differences between model C and D result from the fact that the uniform stoichiometric cloud in model C reacts completely in only about 20 ms, while in model D only 32 kg are consumed in about 65 ms. The hydrogen remaining in the fuel rich regions of the plume in model D will burn off later in the fireball, when the mixing with the ambient air feeds in additional oxidizer but will not contribute to the blast wave. Model C is clearly over-conservative. It is worth noting, that the hemispherical TNT explosion on the ground (model A) is not for certain a conservative approximation to the actual scenario, as the loads for gauge 1 are smaller as with model D. The distributions of peak overpressure and overpressure impulse for model D are presented in figure 2 for the entire domain. Similar plots of the distribution of damage effects can be generated using the built-in SDOF models.

Table 2: Loads at considered gauges for different explosion source models

Gauge	Peak OP [kPa]			Max. OP-impulse [Pa s]		
	1	2	3	1	2	3
Model A	8.1	5.1	2.7	233	206	166
Model B	11.1	5.0	3.2	287	183	145
Model C	12.9	5.9	3.4	330	214	165
Model D	9.5	4.6	2.7	250	190	151

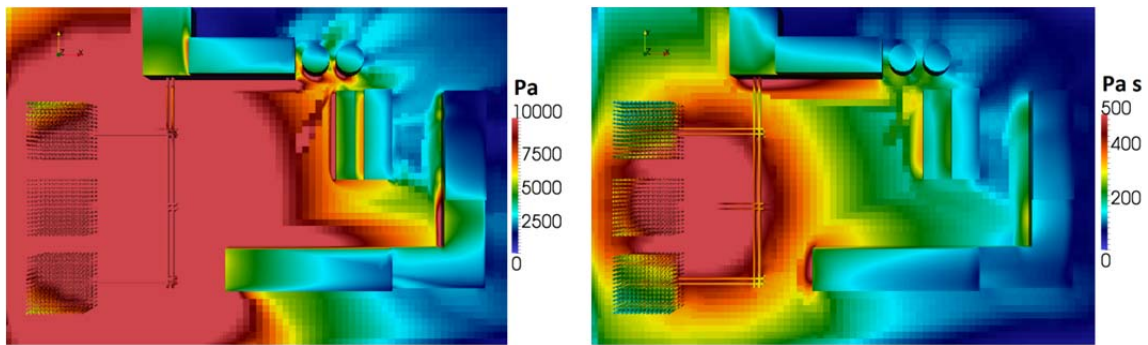


Figure 2: Computed results for model D. Left: distribution of peak overpressure (data clipped at 10 kPa); Right: distribution of maximum overpressure impulse (data clipped at 500 Pa s)

A large number of existing buildings on industrial sites have external masonry walls. A fictitious building of this type has therefore been selected as an example (figure 1). The floor height is 4 m and for the wall width the asymptotic case $width \gg height$ was assumed. The masonry walls are 24 cm thick, the mortar strength is 5 N/mm². Due to the static pre-stress by the weight of the upper floors, the load bearing capacity increases from the top to the ground floor. Static load capacities of 0.48 kPa and 1.23 kPa can be calculated for the walls of the top floor and the ground floor, respectively. Their eigenfrequencies and the duration of the considered loading lead to DLFs of about one for all floors; the static values thus equal the equivalent static loads for the elastic limit. Following Pigler (1976) the masonry walls would withstand a maximum explosion overpressure of 1 kPa. Using the equation from Gilbert, Lees and Scilly (1994) the distance for the lowest damage level D (buildings remain habitable with minor damage) is 285 m and 142 m for the next higher damage level Ca (inhabitable but repairable). The iso-damage curves for the considered walls shown in figure 3 were calculated according to (Fischer, 2009). They are based on the aforementioned values of the static load bearing capacities. Table 3 summarizes the results of the different damage models for the walls at positions 1 to 3

using the explosive loads according to model D. The SDOF model can here be regarded as the most realistic one, as it includes both the wall dynamics and the static pre-stress appropriately. Thereby it permits a differentiated and reliable assessment of the expected damage.

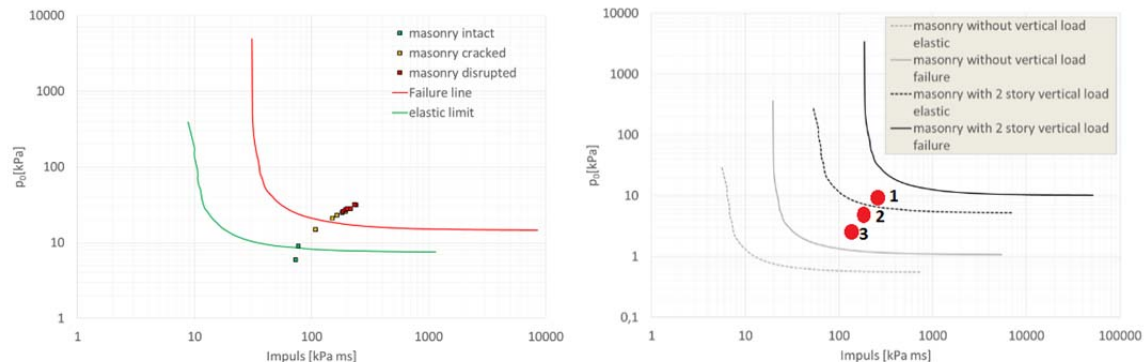


Figure 3: Comparison between experimental data and SDOF predictions for masonry walls (left); Iso-damage curves and loads for the considered 24 cm masonry walls (right): dotted lines indicate the elastic limit, solid lines the failure thresholds; black lines refer to the ground floor, grey lines to the top floor.

Table 3: Evaluation of structural damage for individual walls of the considered building with different models

Wall at	1	2	3	Comment
Pigler	Fail	Fail	Fail	Masonry withstands 1 kPa maximum
Gilbert, Lees, Scilly	Damage	Damage	Damage	Radius between damage level D and Ca
Eqv. stat. load	Fail	Fail	Fail	DLF = 1, design w.r.t. EC6
SDOF	Damage	Intact	Fail	Includes static pre-stress

References

- Baker, Q.A. Tang, M.J., Scheier, E.A. Silva, G.J., 1996, Vapor cloud explosion analysis. Process Safety Progress, vol. 15, (1996), pp. 106–109.
- Committee for the Prevention of Disasters (CPR), 2005, Methods for the calculation of physical effects due to releases of hazardous materials – the yellow book, publication CPR 14E.
- Eurocode 6: design of masonry structures – Part 1-1 General rules for reinforced and unreinforced masonry structures, 2012.
- Fischer, K., Häring, I., 2009, SDOF response model parameters from dynamic blast loading experiments, Engineering Structures, vol. 31, no. 8, pp. 1677-1686.
- Gilbert, S.M., Lees, F.P., Scilly, N.F., 1994, A model for hazard assessment of the explosion of an explosives vehicle in a built-up area, 26th DoD Explosives Safety Seminar, Miami.
- Jarrett, D.E., 1968, Derivation of the British explosives safety distances, Annals of the New York Academy of Sciences, vol. 152.
- Kinney, G.F., Graham, K.J., 1985, Explosive Shocks in Air, Springer-Verlag, New York.
- Klomfass, A., 2014, Modelling and simulation of hydrogen-air detonations and blast waves, Paper presented at the 10th Int. Symp. on hazards, prevention, mitigation of industrial explosions, 2014, Bergen, Norway
- Morison, C., 2006, Dynamic response of walls and slabs by single-degree-of-freedom analysis - a critical review and revision, International Journal of Impact Engineering 32(8), pp. 1214-1247.
- Pigler, F., 1976, Druckbeanspruchung der Schaltanlagenräume durch Störlichtbögen, Energiewirtschaftliche Tagesfragen 26. Jg. (1976) Heft 3.
- Stone, P.D., Henderson, J., 2006, World War II bomb damage, accidental explosions and the basis of our current quantity distances, 32nd Explosives Safety Seminar.
- Stolz, A., Fischer, K., Roller, C., Hauser, S., 2014, Dynamic bearing capacity of ductile concrete plates under blast loading, International Journal of Impact Engineering, Bd. 69, pp. 25-38.
- Teich, M., Gebbeken, N., 2010, The Influence of the Underpressure Phase on the Dynamic Response of Structures Subjected to Blast Loads, International Journal of Protective Structures Volume 1, Number 2.
- Unified Facilities Criteria UFC 3-240-02, 2008, Structures to Resist the Effects of Accidental Explosions, US Department of Defense, US Army Corps of Engineers, Naval facilities Engineering Command, Air Force Civil Engineer Support Agency – 5 December 2008 (replaces ARMY TM5-1300 of November 1990).